Phase diagram and quasiparticles of a lattice SU(2) scalar-fermion model in 2+1 dimensions

J. L. Alonso[1,*] Ph. Boucaud,[2,†] V. Martín-Mayor,[3,‡] and A. J. van der Sijs[4,§]
[1]*Departamento de Física Teórica, Universidad de Zaragoza, 50009 Zaragoza, Spain*
[2]*LPTHE, Université de Paris XI, 91405 Orsay Cedex, France*
[3]*Dipartimento di Fisica and Infn, Università di Roma La Sapienza, P. A. Moro 2, 00185 Roma, Italy*
[4]*Swiss Center for Scientific Computing, ETH-Zürich, ETH-Zentrum, CH-8092 Zürich, Switzerland*
(Received 21 July 1999; published 23 December 1999)

The phase diagram at zero temperature of a lattice SU(2) scalar-fermion model in 2+1 dimensions is studied numerically and with mean-field methods. Special attention is devoted to the strong coupling regime. We have developed a new method to adapt the hybrid Monte Carlo algorithm to the O(3) non-linear σ model constraint. The charged excitations in the various phases are studied at the mean-field level. Bound states of two charged fermions are found in a strongly coupled *paramagnetic* phase. On the other hand, in the strongly coupled antiferromagnetic phase fermionic excitations around momenta $(\pm\pi/2,\pm\pi/2,\pm\pi/2)$ emerge.

PACS number(s): 11.15.Ha, 02.70.Lq, 11.15.Ex, 11.30.Rd

I. INTRODUCTION

The model we are going to study was proposed in Refs. [1] and [2] as a natural extension of the lattice O(3) non-linear σ model in 2+1 dimensions to include charge carriers. It is a lattice model of interacting spins and Dirac fermions in 2+1 dimensions, with only two free parameters in addition to the temperature: a nearest-neighbor spin coupling and a spin-fermion coupling. The model describes quantitatively some of the features of the doped copper oxide compounds [1,2].

In the present article we want to present a careful, detailed discussion of the model, its symmetries, and its properties, and give full technical details and results of the mean-field (MF) and Monte Carlo (MC) calculations, some of which were reported in Ref. [1]. In this paper, our mean-field and numerical studies will be limited to the zero-temperature case, corresponding to infinite Euclidean time direction.

The remainder is laid out as follows. In Sec. II we present our model, discuss the choice of lattice fermions, comment on the symmetries of the model, give its phase diagram and prove the reality of the fermion determinant, even in the presence of a chemical potential. In Sec. III we examine the phase diagram of the model in the MF approximation. Our MF calculations are based on small- and large-y expansions combined with saddle point methods. The method allows us to handle (products of) fermionic variables occurring in the expansion of the fermion determinant in a well defined way. In Sec. IV we use MC simulations to complete the study of the phase diagram. For this purpose we have developed a new method that exactly solves the technical problem related to the length-1 constraint on the spin variables [3]. Section V is devoted to a study of the relevant excitations in the different phases of the system, at the MF level. A crucial result is the dynamical generation of spin singlet bosonic bound states of charged fermions in the so-called paramagnetic strong (PMS) phase. At the MF level we have not found evidence for *fermionic* excitations at *zero* temperature in this PMS phase. Another interesting result is the emergence of fermionic excitations around momenta $(\pm\pi/2,\pm\pi/2,\pm\pi/2)$ in the strongly coupled antiferromagnetic (AFM) phase [4]. Finally, Sec. VI is devoted to our conclusions and projects.

II. THE MODEL: FORMULATION, SYMMETRIES, PHASE DIAGRAM

The model is defined by the following (2+1)-dimensional lattice Euclidean (imaginary time) path integral,

$$Z=\int D\boldsymbol{\phi}D\bar{\psi}D\psi\exp(-S) \tag{1}$$

with the action

$$S=-\sum_{x,\mu}k\boldsymbol{\phi}_x\cdot\boldsymbol{\phi}_{x+\hat{\mu}}+\sum_{x,\mu}\frac{\rho}{2}\bar{\psi}_x\gamma^\mu(\psi_{x+\hat{\mu}}-\psi_{x-\hat{\mu}})+\sum_x\lambda\bar{\psi}_x\boldsymbol{\phi}_x\cdot\boldsymbol{\tau}\psi_x. \tag{2}$$

We use this expression as our starting point, but it should be noted that the model *depends only on the ratio* $y=\lambda/\rho$, *through a change in the normalization of the fermion field*. In terms of the effective spin-fermion coupling y, we get

$$S=-\sum_{x,\mu}k\boldsymbol{\phi}_x\cdot\boldsymbol{\phi}_{x+\hat{\mu}}+\sum_{x,\mu}\frac{1}{2}\bar{\psi}_x\gamma^\mu(\psi_{x+\hat{\mu}}-\psi_{x-\hat{\mu}})+\sum_x y\bar{\psi}_x\boldsymbol{\phi}_x\cdot\boldsymbol{\tau}\psi_x. \tag{3}$$

Here x runs over a (2+1)-dimensional cubic Euclidean space-time lattice. Each ψ_x is a fermionic four-spinor as a shorthand for two flavors of two-component Dirac spinors. Both flavors are taken in the same irreducible spinor repre-

*Email address: buj@gteorico.unizar.es
†Email address: phi@qcd.th.u-psud.fr
‡Email address: Victor.Martin@roma1.infn.it
§Email address: arjan@scsc.ethz.ch

sentation, with 2×2 gamma matrices taken as the Pauli matrices σ^μ. The 4×4 matrices γ^μ in Eq. (3) have the form

$$\gamma^\mu=\begin{pmatrix}\sigma^\mu & 0\\ 0 & \sigma^\mu\end{pmatrix}\qquad \mu=1,2,3. \tag{4}$$

The kinetic term for the fermions is of the nearest-neighbor (hopping) form. Lattice fermions defined in this way undergo species doubling in the perturbative continuum limit [5]. For two reasons we are going to leave this matter aside in this work. First, we are particularly interested in the strong coupling non-perturbative regime where more of the interesting physics occurs [1,2]. In this strong coupling regime all the fermions, the physical one as well as the doublers, decouple in the continuum limit [6]. Second, this model described qualitatively some of the features of the doped copper oxide compounds [1,2], where the lattice space is given by the material.

The three-component $\boldsymbol{\phi}$ are real scalar bosonic variables, subject to the constraint $\boldsymbol{\phi}^2=1$, as in the O(3) non-linear σ model. The last term in Eq. (3) describes the interaction between $\boldsymbol{\phi}$ and the Dirac fermions, which is diagonal in Dirac space. The Pauli matrices τ^a act in flavor space.

Let us now consider the symmetries of Eq. (3). First of all, we have the usual cubic symmetry. Next, there is a discrete parity symmetry, which in $2+1$ dimensions is defined as the reflection of one of the spatial axes, say the x axis. Under this parity symmetry, the fermions can be seen to transform as

$$\psi\to\sigma_1\psi,\qquad \overline{\psi}\to-\overline{\psi}\sigma_1, \tag{5}$$

so $\boldsymbol{\phi}$ is a pseudoscalar in this sense. In addition, the action (3) is invariant under an SU(2) flavor symmetry in which ψ transforms as the fundamental representation and $\boldsymbol{\phi}$ transforms as the adjoint one. Note that by requiring the two fermion flavors to have the same Lorentz structure [that is, by choosing the γ's as in Eq. (4)] no fermion mass term is allowed which preserves the above symmetries [7].

There are two more discrete symmetries of our model (3), which will be useful in the MF calculation of the phase diagram. The first one is

$$Z(k,y)=Z(k,-y), \tag{6}$$

which becomes clear if we make the change of variables

$$\psi_x\to\exp\left(i\frac{\pi}{2}\epsilon_x\right)\psi_x,\qquad \overline{\psi}_x\to\exp\left(i\frac{\pi}{2}\epsilon_x\right)\overline{\psi}_x, \tag{7}$$

where

$$\epsilon_n=(-1)^{\Sigma_\mu x_\mu}. \tag{8}$$

This implies that $Z(k,y)$ is a function of y^2 only and we can restrict ourselves to $y>0$.

In addition, there is a symmetry

$$Z(k,y)=Z(-k,-iy), \tag{9}$$

as can be seen by making the substitutions

$$\psi_x\to\exp\left(i\frac{\pi}{4}\epsilon_x\right)\psi_x,\qquad \overline{\psi}_x\to\exp\left(i\frac{\pi}{4}\epsilon_x\right)\overline{\psi}_x,\qquad \boldsymbol{\phi}_x\to\epsilon_x\boldsymbol{\phi}_x. \tag{10}$$

The latter symmetry implies that the lattice regularization of the non-linear σ model, $y=0$ (or $y=\infty$, see Secs. III, IV), is equally valid in a ferromagnetic or an antiferromagnetic phase.

In order to perform computations in models of this type, one has to integrate out the fermions. This integration leads to a $\boldsymbol{\phi}$-dependent fermion determinant. It is important to know whether this determinant is a real number. To study this, let us write down the original fermion matrix (Latin letters $x,y,\ldots$ will refer to lattice points, $i,j,\ldots$, will represent flavor indices, while Greek letters $\alpha,\beta,\ldots$ are used for Dirac indices):

$$\hat{M}_{x\alpha i;y\beta j}=K_{x\alpha i;y\beta j}+Y_{x\alpha i;y\beta j}, \tag{11}$$

$$K_{x\alpha i;y\beta j}=\frac{1}{2}\sum_\mu\left(\delta_{x+\mu,y}-\delta_{x-\mu,y}\right)\sigma^\mu_{\alpha\beta}\delta_{ij}, \tag{12}$$

$$Y_{x\alpha i;y\beta j}=y\,\delta_{xy}(\boldsymbol{\phi}\cdot\boldsymbol{\tau})_{ij}\delta_{\alpha\beta}. \tag{13}$$

Keeping in mind that for Pauli matrices $\sigma_2\sigma_i\sigma_2=-\sigma_i^*$, where $*$ means complex conjugation, and that $[\boldsymbol{\gamma},\boldsymbol{\tau}]=0$, one easily proves that, for real y,

$$\sigma_2\tau_2(K+Y)\sigma_2\tau_2=-(K^*+Y^*). \tag{14}$$

Therefore,

$$\det(K+Y)=\det(-K^*-Y^*)=[\det(K+Y)]^*, \tag{15}$$

i.e. the determinant is real. Thus, by doubling the number of fermion families, we obtain a positive determinant. Had we introduced a chemical potential, μ, the only change would be the introduction of $e^{\pm\mu}$ on the temporal links of the kinetic matrix [8]. The essential requirement for Eq. (14) to hold (that the only non-real numbers are in $\boldsymbol{\gamma},\boldsymbol{\tau}$) is thus not endangered by the chemical potential and the determinant is still real.

The phase diagram of the model at zero temperature is shown in Fig. 1. Notice that it is very similar to the phase diagram of (chiral) Yukawa models for the electroweak sector of the standard model of elementary particle interactions [9]. At $y=\infty$ and at $y=0$ we recover the non-linear σ model (see Secs. III and IV) with its well known paramagnetic (PM), ferromagnetic (FM) and antiferromagnetic (AFM) phases. At finite y, we expect these phases to extend into the (k,y) plane. One of its most important features is that there are two mutually disconnected paramagnetic phases, one at weak coupling (called PMW) and one at strong coupling (PMS). One sees that the PMW-FM and the PMW-AFM transition lines meet in a point **A**, where this disordered phase ends. In the strong coupling sector of the phase diagram, a similar behavior is found, with the two transition lines meeting at point **B**. This observation means that one

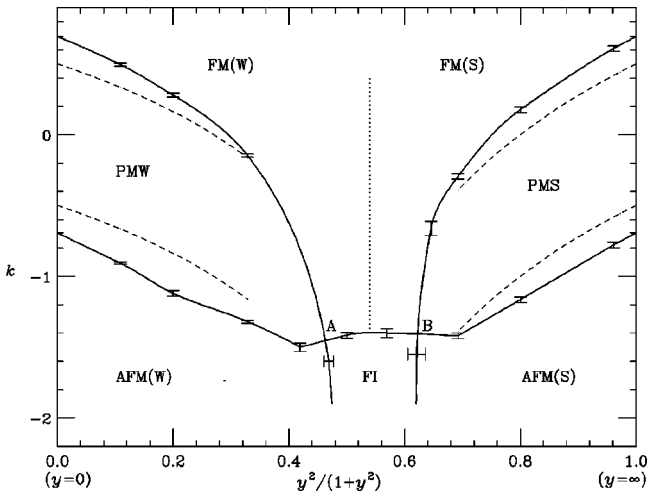

FIG. 1. Phase diagram of the action (3), for two fermion families. Dashed lines are from the MF calculation, solid lines from a MC calculation on an 8^3 lattice.

may expect totally different behavior in each of the two paramagnetic phases. This is indeed the case, as we shall see later.

As there is no evidence for a phase transition between the strong- and weak-coupling regions of the FM and AFM phases, we name them FM(W) and FM(S), AFM(W) and AFM(S) (note the parentheses). There may be crossovers between these regions, though.

Between the points **A** and **B**, we find a phase where both the magnetization and the staggered magnetization are different from zero. We name this phase *ferrimagnetic* (FI). An appealing possibility is that it corresponds to a helicoidal phase. We expect the FI phase to disappear for large enough $-k$, but we have not explored this numerically.

III. MEAN FIELD CALCULATIONS OF THE PHASE DIAGRAM

Our aim in this section is to determine the zero-temperature phase diagram of the model in the y-k plane (cf. Fig. 1), using mean-field techniques. These calculations already provide a lot of insight, especially for the strong coupling region. They will be contrasted with numerical simulations for the phase diagram in Sec. IV, and they will be extended to a study of the relevant charged (quasi-particle) excitations in Sec. V.

Our mean-field calculations are based on small- and large-y expansions combined with the saddle point methods described in Ref. [10]. This approach guarantees a systematic expansion in $1/d$, which is particularly important for operators which are zero to lowest-order. Our particular method furthermore allows us to handle (products of) fermionic variables occurring in the expansion of the fermion determinant in a well defined way. These techniques have been developed and applied in the context of similar lattice models [11,12] of the electroweak sector of the standard model of elementary particle interactions, and in the study of the antiferromagnetic ϕ^4 model [13].

We shall first concentrate on the small-y region, and incorporate the fermion determinant up to $\mathcal{O}(y^2)$.

In order to apply the saddle-point method, the integration over the fields must be unrestricted. We therefore need to replace the integration over the spin vectors $\boldsymbol{\phi}$, constrained by the condition $|\boldsymbol{\phi}|=1$, with an integration over unconstrained variables $\boldsymbol{\xi}$. This is done by multiplying the functional integrand in Eq. (1) by

$$1=\int D\xi\,\delta(\boldsymbol{\phi}-\boldsymbol{\xi})\equiv\prod_n\prod_{a=1}^{3}\int_{-\infty}^{\infty}d\xi_x^a\,\delta(\phi_x^a-\xi_x^a)$$

$$=\prod_x\prod_{a=1}^{3}\int_{-\infty}^{\infty}d\xi_x^a\int_{-\infty}^{\infty}\frac{dA_x^a}{2\pi}\exp[iA_x^a(\phi_x^a-\xi_x^a)],$$

and replacing a conveniently chosen subset of the $\boldsymbol{\phi}$ variables in the action S with $\boldsymbol{\xi}$ fields. We obtain

$$Z=\int\frac{D\xi DA}{(2\pi)^3}\exp\left[k\sum_{x,\mu}\boldsymbol{\xi}_x\cdot\boldsymbol{\xi}_{x+\mu}-i\sum_x\boldsymbol{A}_x\cdot\boldsymbol{\xi}_x\right]$$
$$\times\int D\bar{\psi}D\psi\exp\left[-\sum_{x,\mu}\frac{1}{2}\bar{\psi}_x\gamma^\mu(\psi_{x+\hat{\mu}}-\psi_{x-\hat{\mu}})\right]$$
$$\times\prod_x\left\{\int\frac{d\boldsymbol{\phi}_x}{4\pi}\exp[i\boldsymbol{A}_x\cdot\boldsymbol{\phi}_x-y\bar{\psi}_x\boldsymbol{\phi}_x\cdot\vec{\tau}\psi_x]\right\}. \quad (16)$$

Note that both the $\boldsymbol{\xi}$ fields and the auxiliary fields $\boldsymbol{A}$ are unconstrained.

Now we have to integrate out the constrained variables ϕ_n^a (as well as the fermions), before the mean fields can be introduced. Let us concentrate on a single $\boldsymbol{\phi}_n$ integration in Eq. (16), dropping the subscripts n for simplicity. First, we perform an expansion in powers of y. We can write

$$\int\frac{d\boldsymbol{\phi}}{4\pi}\exp[i\boldsymbol{A}\cdot\boldsymbol{\phi}-y\bar{\psi}\boldsymbol{\phi}\cdot\vec{\tau}\psi]$$
$$=\exp[u(i\boldsymbol{A})]\exp\left[-yQ^a\cdot\langle\phi^a\rangle_{i\boldsymbol{A}}+\frac{1}{2}y^2Q^aQ^bT^{ab}\right.$$
$$\left.+\mathcal{O}(y^3)\right], \quad (17)$$

where we have defined

$$Q^a=\bar{\psi}\tau^a\psi,\quad u(i\boldsymbol{A})=\ln\int\frac{d\boldsymbol{\phi}}{4\pi}\exp[i\boldsymbol{A}\cdot\boldsymbol{\phi}],$$

$$T^{ab}=\langle\phi^a\phi^b\rangle_{i\boldsymbol{A}}-\langle\phi^a\rangle_{i\boldsymbol{A}}\langle\phi^b\rangle_{i\boldsymbol{A}},$$

and we have introduced the notation

$$\langle O\rangle_{i\boldsymbol{A}}=\int\frac{d\boldsymbol{\phi}}{4\pi}O\exp[i\boldsymbol{A}\cdot\boldsymbol{\phi}]\Big/\int\frac{d\boldsymbol{\phi}}{4\pi}\exp[i\boldsymbol{A}\cdot\boldsymbol{\phi}].$$

In addition, we introduce a Hubbard-Stratonovich vector parameter $\boldsymbol{\lambda}$ to deal with the quartic fermion term in Eq. (17),

$$\exp\left[\frac{1}{2}y^2\sum_{a,b} Q^a Q^b T^{ab}\right]$$

$$= \int \frac{d\boldsymbol{\lambda}}{(2\pi)^{3/2}} \exp\left[-\frac{1}{2}\sum_a \lambda^a\lambda^a\right]$$

$$\times \exp\left[y\sum_{ab} (\sqrt{T})^{ab} Q^a \lambda^b\right]. \tag{18}$$

(Note that the matrix T is self-adjoint, and positive definite if $\boldsymbol{A}$ is imaginary, so the square root is well defined). Thus, up to this order in y^2, the action is bilinear in the fermion fields.

Carrying out the fermion integration in Eq. (16) now gives $\det M$, where

$$M_{x,\alpha,i;y,\beta,j} = K_{x,\alpha,i;y,\beta,j} + y\,\delta_{xy}\delta_{\alpha\beta}\sum_a \left[\langle \phi_x^a\rangle_{iA_x} - \sum_b (\sqrt{T_x})^{ab}\lambda^b\right]\tau_{ij}^a. \tag{19}$$

The matrix K has been defined in Eq. (12).

The mean fields are the field values at the saddle point of the free energy

$$-F = \sum_x u(i\boldsymbol{A}_x) + k\sum_{x,\mu} \boldsymbol{\xi}_x\cdot\boldsymbol{\xi}_{x+\mu} - i\sum_x \boldsymbol{A}_x\cdot\boldsymbol{\xi}_x - \frac{1}{2}\sum_x \boldsymbol{\lambda}_x^2 + \mathrm{Tr}\log M. \tag{20}$$

A choice of the mean fields should be done at this point, as we cannot calculate $\log M$ for general $\{\boldsymbol{A}_x, \boldsymbol{\lambda}_x\}$. An appropriate choice for the study of a PM-FM phase transition is

$$\boldsymbol{A}_x = (0,0,-i\alpha), \tag{21}$$

$$\boldsymbol{\xi}_x = (0,0,v),$$

$$\boldsymbol{\lambda}_x = (0,0,\lambda),$$

in terms of which (N is the lattice volume)

$$F/N = -u(\alpha) - kdv^2 + \alpha v + \frac{1}{2}\lambda^2 - \frac{1}{N}\mathrm{Tr}\log M, \tag{22}$$

with α, v and λ satisfying the saddle point equations

$$\nabla F|_{(\alpha,v,\lambda)} = 0. \tag{23}$$

The fermion matrix, $M(\alpha,v,\lambda)$, can be calculated in momentum space, where it is diagonal in its momentum indices. One easily finds

$$\det M = \exp\left[2\sum_p \log \frac{\sum_{\mu=1}^3 \sin^2 p_\mu + y^2(u'(\alpha) - \lambda\sqrt{u''(\alpha)})^2}{\sum_{\mu=1}^3 \sin^2 p_\mu}\right], \tag{24}$$

where we have divided out the determinant for free fermions. We need only the leading $\mathcal{O}(y^2)$ contribution to the exponent, hence the mean field free energy becomes, in the infinite volume limit:

$$F/N = -u(\alpha) - kdv^2 + \alpha v + \frac{1}{2}\lambda^2 - 2y^2(u'(\alpha) - \lambda\sqrt{u''(\alpha)})^2 C_0, \tag{25}$$

where

$$C_0 = \int_{-\pi}^{\pi} \frac{d^3p}{(2\pi)^3} \frac{1}{\sum_{\mu=1}^3 \sin^2 p_\mu} = 1.010924\ldots. \tag{26}$$

Incidentally, the above integral can be explicitly solved (see Ref. [14]).

Next, we shall discuss the actual solutions to Eqs. (23). From $u(\alpha) = \ln(\sinh\alpha/\alpha)$, one easily finds that $\alpha = v = \lambda = 0$ always fulfill them. For small k, y, it is a true minimum of the free energy. This characterizes a paramagnetic (PM) phase, since none of the fields develops an expectation value.

For larger values of k and y, there is another, non-trivial solution, corresponding to a ferromagnetic (FM) phase. It emerges when a negative mode in F/N starts to develop, as a function of the mean fields, and the transition between the two regions is given by the condition (F'' is the Hessian matrix)

$$\det F''|_{(\alpha=0,v=0,\lambda=0)} = 0. \tag{27}$$

This condition is satisfied for F/N of Eq. (25) if

$$k = \frac{3}{2d} - \frac{2C_0}{d}y^2. \tag{28}$$

This curve defines the phase transition line between the PM and FM phases in the small-y region. Using the symmetry (9), we deduce that there is a similar transition separating the PM and AFM phases,

$$k = -\frac{3}{2d} - \frac{2C_0}{d}y^2. \tag{29}$$

Let us finally remark that in the presence of N_f such fermion fields we would have N_f factors of $\det M$, leading to a multiplication of C_0 by N_f in Eqs. (28) and (29).

The large-y region is easier to deal with. Here it is convenient to integrate out the fermions directly in Eq. (16), leading to (summation over repeated index is carried)

$$\det M_{x,\alpha,i;y,\beta,j}$$

$$= \det\left(K_{x,\alpha,i;y,\beta,j} + y\,\delta_{\alpha\beta}\delta_{xy}\sum_a \phi_x^a \tau_{ij}^a \right) \tag{30}$$

$$= \det\left(y\,\delta_{\alpha\gamma}\delta_{xz}\sum_a \phi_x^a \tau_{ik}^a \right)$$

$$\times \det\left(\delta_{zy}\delta_{\gamma\beta}\delta_{kj} + \frac{1}{y}\sum_b \phi_z^b \tau_{kl}^b K_{z,\gamma,l;y,\beta,j} \right). \tag{31}$$

Here we have used that $(\Sigma_a \phi^a \tau^a)^2 = \mathbb{1}$ (recall the $\boldsymbol{\phi}$'s are unit vectors). Now we can expand $\log(\det M)$ in powers of $1/y$. The $\mathcal{O}(1/y)$ term vanishes by virtue of $K_{xx}=0$. To second order one obtains

$$\log\det M = \log y^{4N} + \mathrm{Tr}\left(-\frac{1}{2y^2}\sum_a \phi_x^a \tau_{ki}^a K_{x\alpha i;t\gamma l} \times \sum_b \phi_t^b \tau_{lj}^b K_{t\gamma j;y\beta p} \right) \tag{32}$$

$$= \log y^{4N} + \frac{1}{y^2}\sum_{x,\mu} \boldsymbol{\phi}_x \cdot \boldsymbol{\phi}_{x+\hat{\mu}}. \tag{33}$$

Here, $\log y^{4N}$ is an irrelevant constant that can be dropped. Notice also that this expression will acquire a prefactor N_f if there are N_f identical fermion flavors. One sees that, up to $\mathcal{O}(1/y^2)$, the only effect of the fermion determinant is a renormalization of the scalar hopping parameter of the O(3) model,

$$k \to k + N_f \frac{1}{y^2}. \tag{34}$$

Note that we did not introduce any mean fields to derive this result. The usual MF treatment of the O(3) model with this renormalized coupling now immediately gives us the required phase transition lines in the large-y region of our model:

$$k = \pm\frac{3}{2d} - N_f\frac{1}{y^2}. \tag{35}$$

It is interesting to compare the small- and large-y results, to leading order in $1/d$. As is well known, the first order in this expansion is equivalent to any MF approximation, up to higher-order terms. For this purpose, we need the $1/d$ expansion of the constant C_0 in Eq. (26), which can be calculated as follows:

$$C_0(d) = \int_{-\pi}^{\pi} \frac{d^d p}{(2\pi)^d} \frac{1}{\sum_{\mu=1}^{d} \sin^2 p_\mu} = 2\int_0^\infty ds\,(e^{-s} I_0(s))^d \tag{36}$$

$$= \frac{2}{d}\left(1 + \frac{1}{2d} + \mathcal{O}\left(\frac{1}{d^2}\right) \right), \tag{37}$$

where $I_0(s) = \int_{-\pi}^{\pi} (d\theta/2\pi)\exp(s\cos\theta)$ is the modified Bessel function. In fact, the second equality in Eq. (36) was used to obtain the numerical result (26) for C_0.

Keeping only the leading-order term $2/d$ for C_0 we find that the phase transition lines would meet at $y^2 = 2/d$.

Now we are ready to map out the phase diagram of the model, as predicted by the MF method for the weak and strong coupling regions. This is done in Fig. 1. The vertical axes at $y=0$ and $y=\infty$ correspond to the O(3) model, with its disordered (PM) and ordered (FM and AFM) phases. These phases extend into the y direction, both for $y>0$ and $y<\infty$. Note that all the phase transition lines bend downward. This can be understood intuitively by assuming a MF value for the fermion condensate, which would act as an external field tending to align the spins ϕ in parallel.

IV. MONTE CARLO ALGORITHM: METHOD AND RESULTS

A well established method for dynamical fermion simulations is hybrid Monte Carlo (HMC) algorithm [15]. However, the implementation of this algorithm in a model with constrained variables is not straightforward. This has been satisfactorily achieved for models with variables belonging to a Lie group [16], such as SU(N) gauge theories or some spin models, such as the O($N=2,4$) non-linear σ models. However, for other spin variables (not in a Lie group), as in the O(3) non-linear σ model, this had not been satisfactorily solved yet, although the problem arose already in the first simulations using the Langevin algorithm [3]. Our solution is a generalization of the strategy in [16].

We shall first discuss our solution in the quenched approximation, where comparison with other algorithms is possible (Sec. IV A), and then deal with the full theory in Sec. IV B. Finally our Monte Carlo results for the phase diagram of the full theory will be presented in Sec. IV C.

A. The HMC method for the quenched approximation

For the purpose of discussion it will prove convenient to briefly describe the HMC method for unconstrained bosonic variables $\phi(x)$ with action $S_B(\phi)$ (see Ref. [17] for a pedagogical presentation):

(1) Introduce uncorrelated Gaussian variables $\pi(x)$ of unit variance (the *conjugate momenta* for the fields ϕ) and define a Hamiltonian

$$H = \sum_x \frac{1}{2}\pi^2(x) + S_B(\phi). \tag{38}$$

One can then use the Hamiltonian equations of motion

$$\dot{\phi}(x,\tau)=\pi(x,\tau),$$

$$\dot{\pi}(x,\tau)=-\frac{\delta S_B}{\delta\phi(x,\tau)}, \tag{39}$$

to perform a microcanonical molecular dynamics evolution in ''Monte Carlo time,'' τ. After a certain period of MC time (called ''trajectory''), new random momenta $\pi(x)$ are chosen (''refreshing'' the momenta). The crucial properties of Eqs. (39) are their time reversibility, and the invariance of the Liouville measure, $D\phi\, D\pi$, under time evolution.

(2) In practice, the molecular dynamics equations of motion for a trajectory are discretized into N steps $\Delta\tau$. This is done using a leap-frog algorithm which is *exactly* time reversible, but does introduce a systematic error which shows up as a non-zero $\Delta H=\mathcal{O}(\Delta\tau^2)$. The *detailed-balance* is not endangered by this error, because a Metropolis acceptance step is performed. For fixed trajectory length, N can then be tuned to optimize the overall efficiency.

To generalize the method to constrained variables, one needs to appropriately define the conjugate momenta and the equations of motion in order to preserve the constraint and, most importantly, not to spoil the time reversibility. Each spin variable, $\boldsymbol{\phi}$, lives on the surface of a two-sphere, and correspondingly one could imagine an algorithm with two independent conjugate momenta, maybe living in the perpendicular plane ($\boldsymbol{\phi}\cdot\boldsymbol{\pi}=0$). However, changing the constraint from the field $\boldsymbol{\phi}$ to the momenta is not very appealing (and, from the practical side, one would need to worry about *two* constraints in the numerical integration). A different approach, the use of spherical coordinates, has the drawback of a non-planar integration measure. Our very simple algorithm avoids constraints and non-planar measures, by introducing *three* conjugate momenta per spin.

We shall start from an analogy with the dynamics of a particle living in the sphere, a potential (V) acting on it. The Hamiltonian is

$$H^{\text{sphere}}=\frac{\boldsymbol{L}^2}{2}+V(\boldsymbol{\phi}). \tag{40}$$

Here $\boldsymbol{L}$ is the angular momentum, $\boldsymbol{\phi}\times\dot{\boldsymbol{\phi}}$. The equations of motion can now be obtained from the Poisson Bracket [18] with the Hamiltonian (40):

$$\dot{\boldsymbol{\phi}}=\boldsymbol{L}\times\boldsymbol{\phi},\quad \dot{\boldsymbol{L}}=-\boldsymbol{\phi}\times\frac{\delta V}{\delta\boldsymbol{\phi}}. \tag{41}$$

In this expression $\delta V/\delta\boldsymbol{\phi}$ stands for $(\delta V/\delta\phi_1,\delta V/\delta\phi_2,\delta V/\delta\phi_3)$.

This formalism is still inconvenient for us, because the constraint $\boldsymbol{\phi}\cdot\boldsymbol{L}=0$ complicates the generation of random momenta according to a Gaussian distribution. However, the following simple facts can be straightforwardly established from Eq. (41):

(I) Both $\boldsymbol{\phi}^2$ and $\boldsymbol{\phi}\cdot\boldsymbol{L}$ are conserved through the time evolution. If the initial condition verifies the constraints $\boldsymbol{\phi}^2=1,\boldsymbol{\phi}\cdot\boldsymbol{L}=0$, this will not be spoiled by the dynamics.

(II) The dynamics is time-reversible.

(III) Although the L_i cannot be all canonical variables [18], the ''Liouville'' measure, $D\boldsymbol{\phi}D\boldsymbol{L}$ $(=d\phi_1 d\phi_2 d\phi_3 dL_1 dL_2 dL_3)$, is left invariant by the time evolution.

(IV) The Hamiltonian is a constant of the motion.

Now let us forget about the constraint $\boldsymbol{\phi}\cdot\boldsymbol{L}=0$, i.e., we introduce a new field $\boldsymbol{P}$ which can have a ''radial component'' (it is no longer an angular momentum), but we keep the equations of motion (41). Obviously, statements I–IV will still hold. Whether a symplectic structure is hidden under this new dynamical system is unclear, but also irrelevant (properties II and III are the essential ones for HMC to be a correct algorithm [17]).

So, we introduce three momenta per spin, $\boldsymbol{P}=(P_1,P_2,P_3)$, and write down the Hamiltonian

$$H=\sum_x \frac{\boldsymbol{P}^2}{2}+S_B(\boldsymbol{\phi}). \tag{42}$$

Equations of motion respecting properties I–IV are easily generalized:

$$\dot{\boldsymbol{\phi}}_{(x,\tau)}=\boldsymbol{P}_{(x,\tau)}\times\boldsymbol{\phi}_{(x,\tau)},\quad \dot{\boldsymbol{P}}_{(x,\tau)}=-\boldsymbol{\phi}_{(x,\tau)}\times\frac{\delta S_B}{\delta\boldsymbol{\phi}_{(x,\tau)}}. \tag{43}$$

As expected, the evolution equations for the S^2 fields ϕ take the form of (infinitesimal) rotations, while the conjugate momenta can be considered as living in the Lie algebra of SO(3). The discretized leap-frog form of these equations is therefore naturally formulated in terms of finite SO(3) rotations,

$$\boldsymbol{\phi}_x(n\Delta\tau+\Delta\tau)=\exp\left[\Delta\tau\boldsymbol{P}_x\left(\left(n+\frac{1}{2}\right)\Delta\tau\right)\cdot\boldsymbol{J}\right]\boldsymbol{\phi}_x(n\Delta\tau), \tag{44}$$

$$\boldsymbol{P}_x\left(\left(n+\frac{1}{2}\right)\Delta\tau\right)=\boldsymbol{P}_x\left(\left(n-\frac{1}{2}\right)\Delta\tau\right)-\boldsymbol{\phi}_{(x,n\Delta\tau)}\times\frac{\delta S_B}{\delta\boldsymbol{\phi}_{(x,n\Delta\tau)}}\Delta\tau, \tag{45}$$

where $\boldsymbol{J}$ are the 3×3 generators of SO(3), satisfying

$$(\exp[\theta\boldsymbol{n}\cdot\boldsymbol{J}])_{ij}=\delta_{ij}\cos\theta+n_i n_j(1-\cos\theta)-\epsilon_{ijk}n_k\sin\theta \tag{46}$$

for unit vectors n. Again, the length constraint on the ϕ fields is preserved by construction.

This final result is reminiscent of the elegant solution for models with variables belonging to a Lie group and conjugate momenta in the group algebra (or vice versa) [16].

In our case, $S_{B\ \text{quenched}}=-k\Sigma_{n,\mu}\boldsymbol{\phi}_n\cdot\boldsymbol{\phi}_{n+\hat{\mu}}$, so the HMC algorithm can now be implemented in a straightforward manner. To test the algorithm, we have simulated the O(3) model on an 8^3 lattice at $k=0.693\approx k_c$ [20] with our HMC

TABLE I. Values for several observables in the quenched model (3) on an 8^3 lattice at $k=0.693\approx k_c$, obtained with our implementation of HMC and with Wolff's single cluster algorithm [19].

Algorithm	$\langle E\rangle$	$\partial_k\langle E\rangle$	χ/V	ξ	B
HMC	0.3505(5)	1.51(2)	0.1426(9)	4.47(2)	0.800(6)
Wolff	0.35061(13)	1.501(10)	0.1432(2)	4.486(9)	0.8031(18)

algorithm and with Wolff's single-cluster embedding algorithm [19]. Let us first define the measured observables, and then compare them.

In this work we have only measured bosonic observables, as our sole objective was the numerical determination of the phase diagram. We have constructed our observables in terms of the Fourier transform of the spin field:

$$\hat{m}(\boldsymbol{p})=\frac{1}{V}\sum_x \exp(-i\boldsymbol{p}\cdot\boldsymbol{x})\boldsymbol{\phi}_x, \tag{47}$$

where $V=L^3$ is the lattice volume.

We define the non-connected finite-volume susceptibilities as

$$\chi=V\langle\hat{m}^2(0,0,0)\rangle, \quad \chi_s=V\langle\hat{m}^2(\pi,\pi,\pi)\rangle. \tag{48}$$

The subscript ''s'' on χ_s stands for ''staggered,'' and this term is used to label quantities which are taken with a weight -1 for the odd lattice sites, corresponding to momentum (π,π,π). Notice that χ/V is a pseudo order parameter, which should be of order one in a ferromagnetically broken phase, and of order $1/V$ in a paramagnetic or antiferromagnetic phase (and similarly for χ_s/V).

Another quantity of interest is the Binder cumulant

$$B=\frac{5}{2}-\frac{3}{2}\frac{\langle(\hat{m}^2(0,0,0))^2\rangle}{\langle\hat{m}^2(0,0,0)\rangle^2}, \tag{49}$$

with an analogous definition for the staggered variant B_s.

One expects $B=1$ in the FM phase, where χ/V is non-vanishing in the thermodynamic limit, while it should be of order $1/V$ in the PM phase, far from the phase transition.

For the correlation length, we use a definition which is easy to measure and gives accurate results:

$$\xi=\left(\frac{\chi/F-1}{4\sin^2(\pi/L)}\right)^{1/2}, \tag{50}$$

where F is the squared Fourier transform at minimal non-zero momentum,

$$F=\frac{V}{3}(\langle|\hat{m}(2\pi/L,0,0)|^2\rangle+\text{permutations}). \tag{51}$$

Again, the generalization to staggered quantities is straightforward. Another kind of observable, needed for the standard extrapolation method [21], is the normalized nearest-neighbor energy

$$E=\frac{1}{3V}\sum_{x,\mu}\langle\boldsymbol{\phi}_x\cdot\boldsymbol{\phi}_{x+\hat{\mu}}\rangle=\frac{\partial}{\partial k}\ln Z. \tag{52}$$

We also measure its fluctuation, given by

$$3V(\langle E^2\rangle-\langle E\rangle^2)=\frac{\partial}{\partial k}\langle E\rangle. \tag{53}$$

In Table I we compare the values obtained for these observables, using our HMC algorithm and the single-cluster algorithm. We find excellent agreement. Of course the efficiency of our implementation of HMC is not competitive with a cluster method in the O(3) non-linear σ model. But it could be useful in other models where cluster methods are not effective in reducing the dynamical critical exponent z (for instance, when some kind of frustration is present [22]), while HMC is expected to yield $z=1$ for any bosonic model.

B. The HMC algorithm for the full theory

The only restriction imposed on HMC is that the fermion bilinear in the action should be given in terms of a positive definite matrix. This will be the case if we consider two identical fermion families ($N_f=2$) as is usually done in lattice gauge theories. After integrating them out we obtain $(\det\hat{M})^2=\det(\hat{M}^\dagger\hat{M})$, where $\hat{M}$ is the fermion matrix for a single fermion family. As we are mainly interested in the strong spin-fermion coupling region, it makes sense to perform the following manipulation:

$$\det\hat{M}=\det(Y+K)=y^{4V}\det(1+Y^{-1}K) \tag{54}$$

[cf. Eqs. (30),(31)]. The constant factor y^{4V} can be dropped, and we define $M=1+Y^{-1}K$.

Next, one re-exponentiates the (inverse) fermion matrix by introducing the so-called *pseudo-fermions* z_x, which are complex four-component c-number fields. The partition function is then

$$Z=\int D\boldsymbol{\phi}\,D\bar{z}\,Dz\,\exp(-S_B-\bar{z}(M^\dagger M)^{-1}z). \tag{55}$$

For further details we refer to Ref. [17].

Now the HMC Hamiltonian becomes

$$H=\sum_x\frac{1}{2}\boldsymbol{P}_x^2-k\sum_{x,\mu}\boldsymbol{\phi}_x\cdot\boldsymbol{\phi}_{x+\mu}+z^\dagger(M^\dagger M)^{-1}z, \tag{56}$$

and the time reversible, constraint and energy preserving equations of motion are

TABLE II. Comparison of observables in the full theory (3) at $(k=0.693, y=10.0)$ and in the quenched model both at the corresponding value of $k^{\rm eff}$ and at $k_c=0.693$. We have 140 000 unquenched trajectories $(N=10, \Delta\tau=0.3)$ on a 4^3 lattice. The Metropolis acceptance rate was 65–70 %, with an autocorrelation time of 3–4 trajectories.

Couplings	$\langle E\rangle$	$\partial_k\langle E\rangle$	χ/V	ξ
$k=0.693$, $y=10.0$	0.4164(6)	1.134(6)	0.3111(7)	2.378(4)
$k=0.713$, $y=0$	0.41584(14)	1.130(4)	0.3108(2)	2.3779(18)
$k=0.693$, $y=0$	0.3928(3)	1.174(4)	0.2836(4)	2.214(2)

$$\dot{\boldsymbol{\phi}}_{(x,\tau)} = \boldsymbol{P}_{(x,\tau)} \times \boldsymbol{\phi}_{(x,\tau)}, \tag{57}$$

$$\dot{\boldsymbol{P}}_{(x,\tau)} = -k\sum_{\mu} (\boldsymbol{\phi}_{(x+\mu,\tau)} + \boldsymbol{\phi}_{(x-\mu,\tau)})\boldsymbol{\phi}_{(x,\tau)} - z^{\dagger}(M^{\dagger}M)^{-1}\left[\left(\frac{\delta M^{\dagger}}{\delta \boldsymbol{\phi}_{(x,\tau)}} \times \boldsymbol{\phi}_{(x,\tau)}\right) M + \text{H.c.}\right] \times (M^{\dagger}M)^{-1} z.$$

For the inversion of the fermionic matrix, we have employed the conjugate gradient algorithm. To formulate the stopping criterium, let us define $h=(M^{\dagger}M)^{-1}z$, h_n being the $n^{\rm th}$ trial solution. We continued the conjugate gradient iteration until

$$\frac{|(M^{\dagger}M)h_n - z|^2}{|h_n|^2} \leq R. \tag{58}$$

In the simulation, we need the inverse matrix both for the leap-frog and for the Metropolis accept-reject step. It is clear that R does not need to be the same in both cases. For the Metropolis step, lack of accuracy in the inversion will bias the simulation. To control this, we have checked that the Creutz parameter $\langle\exp(-\Delta H)\rangle$ equals 1 within errors. In some regions of parameter space R values as small as 10^{-25} were needed. The essential requirement on the leap-frog is full reversibility in the numerical integration of the equations of motion (up to the numerical precision reachable with 64-bit floating point arithmetic). As first noticed in Ref. [23], this has no relation with R if the seed for the conjugate-gradient algorithm is chosen to depend on the *actual* configuration only ($h_0=z$, for instance). However, if R is too large, the numerical integration will produce large changes in the Hamiltonian, and the Metropolis acceptance will be poor. We have found that $R=10^{-7}$ during the leap-frog steps allows for a 50% acceptance.

In a first implementation of a new MC algorithm, some consistency checks are extremely useful. In addition, there are three parameters to be adjusted for optimal performance, N, τ and R. We have carried out the following tests:

(1) We have explicitly checked reversibility of the leap-frog algorithm.

(2) We have checked that $\langle\exp(-\Delta H)\rangle=1$ within errors.

(3) The gaussian expectation values, $\langle z^{\dagger}(M^{\dagger}M)^{-1}z\rangle=4$ and $\langle \boldsymbol{P}^2\rangle=3$ have been checked.

(4) We have checked that $\Delta H\propto(\Delta\tau)^2$ in the leap-frog integration, for constant trajectory length $N\Delta\tau$.

In addition, we compared simulation results for the full theory at (k,y), with the output of a quenched simulation at the corresponding effective coupling value obtained in a large-y expansion,

$$k^{\rm eff} = k + \frac{2}{y^2} + O\left(\frac{1}{y^4}\right) \tag{59}$$

[cf. Eq. (34)]. In Table II, we give the mean value of several operators as obtained on a 4^3 lattice at $k=0.693$, $y=10.0$ and in the quenched theory. The agreement is excellent. Notice that even if the shift in the effective coupling is only 3%, the effects of the dynamical fermions can be clearly measured as the observables change quite significantly at the critical point $k_{\rm c}=0.693$.

C. Phase diagram

The phase diagram in Fig. 1 was obtained on an 8^3 lattice. As there is no true phase transition on a finite lattice, a criterium is needed to locate the phase boundaries. We looked for the point where the relevant Binder cumulant equals the value $B=0.8$ it has at $(k=\pm 0.693\approx k_{\rm c}, y=0)$. Since $B=1$ deep in the broken phase and $B\propto 1/L^3$ in the symmetric one, this provides a clean quantitative criterium which yields a point definitely inside the critical region. The width of the critical region decreases as $L^{-1/\nu}$, therefore the systematic error in the critical coupling will be at most of order 10^{-1}. However, since the Binder parameter is a universal quantity, which should stay constant along much of the critical lines, the error rather goes as $L^{-(\omega+1/\nu)}$ [i.e. $\mathcal{O}(10^{-2})$]. Thus, this systematic error is under control in the full theory as well. We used the standard reweighting method [21] to determine the precise location of the points where $B=0.8$.

The total simulation time was 16 days of the 32 Pentium Pro processor parallel computer RTNN based in Zaragoza. To allow for a correct thermalization, we discarded 100 integrated autocorrelation times of the relevant susceptibility. This may look utterly conservative, and the MC history indeed seems to stabilize long before that. However, not much is known about the *exponential* autocorrelation time of fermionic algorithms and one should be cautious.

As Eq. (54) shows, both at $y=\infty$ and at $y=0$ we recover the non-linear σ model with its well known paramagnetic, ferromagnetic and antiferromagnetic phases. At finite y, we expect these phases to extend into the (k,y) plane. In fact

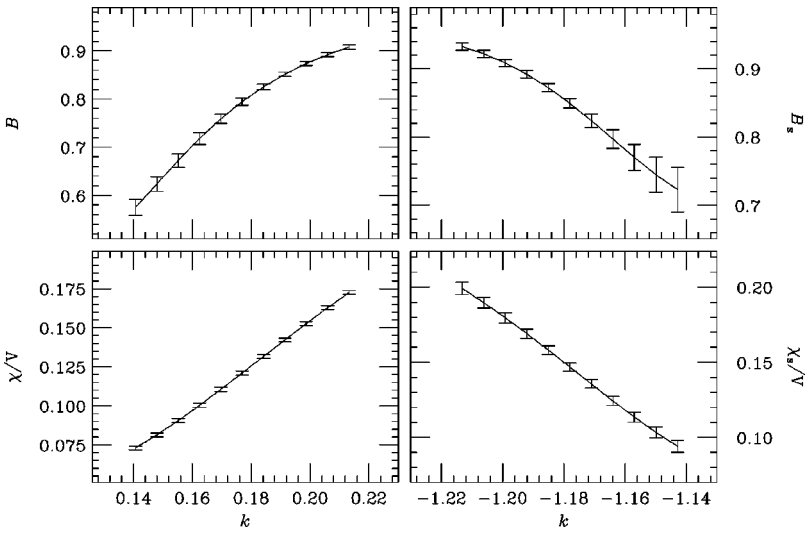

FIG. 2. Binder cumulant (49) and non-connected susceptibility (48) as a function of k, around the two critical points at $y=2.0$. For each critical point, only one simulation has been carried out. The other points are obtained with the standard reweighting method.

one can quite precisely anticipate the critical coupling from the strong coupling formula (59) and the quenched critical points $k_c^{(y=\infty)}=\pm 0.693$. Using the reweighting method, the phase transition lines can be determined down to $y\approx 2.0$. In Fig. 2 the variation of the Binder cumulant and the susceptibility around the two critical couplings is shown for $y=2.0$.

In the small-y region, the effective action up to $\mathcal{O}(y^2)$ does not only renormalize k, but also introduces additional couplings, due to the non-locality of the matrix K^{-1} occurring in the weak-coupling expansion. Therefore, we do not have an estimate for k^{eff} as reliable as in the large-y region (59), but we can nevertheless obtain an estimate for $k_c(y)$ from the MF approximation. We have simulated at several values of the coupling k, for fixed y, until the corresponding Binder parameter crossed its critical value. A more accurate result for the critical point was later on obtained with the reweighting method. In Fig. 3, we have plotted the relevant Binder parameter and susceptibility for k values near the two critical couplings with $y=0.5$.

In Fig. 4 we show the variation of both order parameters and Binder cumulants when crossing the FM(S)-FI transition line at $y=1.15$. We find a strong change in the staggered quantities, while the non-staggered ones show a smoother evolution. However, the non-staggered order parameter is much smaller than its staggered counterpart. This may indicate that, although the non-staggered sector is non-critical ($B\sim 1$), it will eventually undergo a phase transition at lower k. A similar behavior is found when traversing the AFM(W)-FI line at $k=-1.6$ (see Fig. 5), but now the non-staggered quantities show a more pronounced signal. The detailed study of these transition lines (order of the phase transitions, critical exponents, etc.) requires a finite-size scaling analysis, which is left for future work. This study will be much easier if the transition line is crossed varying k, as we lack an analogue of the reweighting method for y.

V. QUASIPARTICLE EXCITATIONS AT THE MF LEVEL

In this section we explore the relevant excitations involving fermions, with emphasis on the strong-coupling region of our model.

The small-y regime has been studied in relation with the mechanism by which leptons and quarks acquire their mass

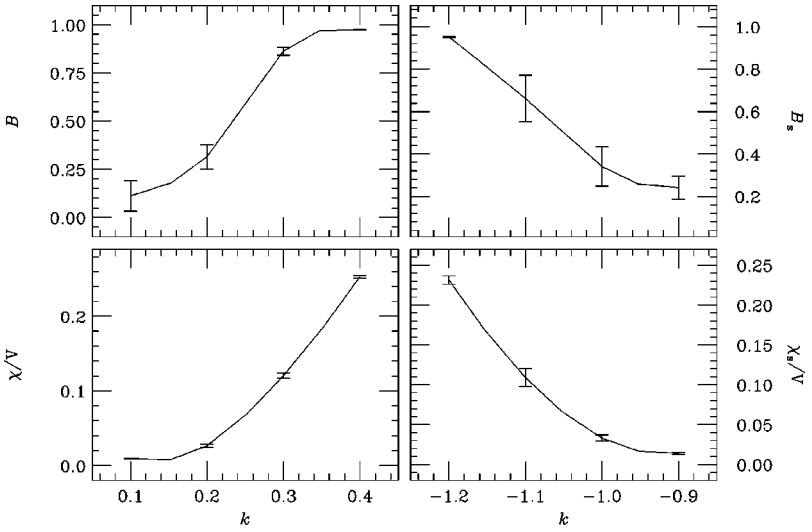

FIG. 3. Binder cumulant (49) and non-connected susceptibility (48) as a function of k, around the two critical points at $y=0.5$. The data points are from different simulations.

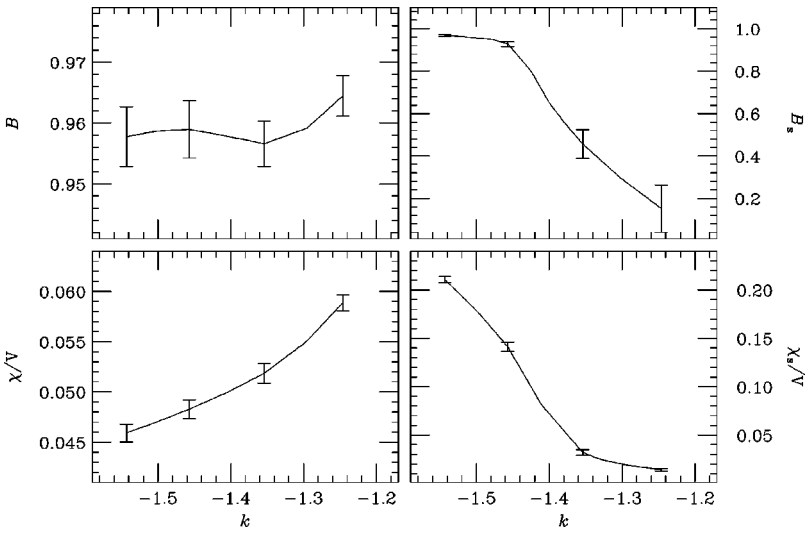

FIG. 4. Binder cumulants and susceptibilities when crossing the FM(S)-FI transition line at $y=1.15$.

through symmetry breaking in the electroweak sector of the standard model. Due to the weak coupling there are no surprises. This situation will change dramatically when we consider the strong-coupling region, though.

A. Fermionic excitations in the FM(S) and PMS phases

At very large y, it is natural to attempt a large-y expansion. This can be achieved after carrying out the following change of variables:

$$\overline{\psi}' = \overline{\psi}, \tag{60}$$

$$\psi' = (\boldsymbol{\phi}\cdot\boldsymbol{\tau})\psi. \tag{61}$$

Because of the constraint $\boldsymbol{\phi}^2=1$ and the identity $(\boldsymbol{\phi}\cdot\boldsymbol{\tau})^2 = \boldsymbol{\phi}^2\mathbf{1}$, this transformation has unit Jacobian and its inverse satisfies

$$\psi = (\boldsymbol{\phi}\cdot\boldsymbol{\tau})\psi'. \tag{62}$$

In terms of the new variables (dropping the primes) the action takes the form

$$S = -k\sum_{x,\mu} \boldsymbol{\phi}_x\cdot\boldsymbol{\phi}_{x+\mu} + \sum_{x,y} \overline{\psi}_x(K_{xy}(\boldsymbol{\phi}_y\cdot\boldsymbol{\tau}) + y\,\delta_{xy})\psi_y\,, \tag{63}$$

where the fermion kinetic term is the usual lattice kinetic Dirac operator, defined in Eq. (12). After a further rescaling of the ψ fields, the coupling y can be moved to the kinetic term, where it appears as $1/y$.

Note that this change of variables (60),(61) was implicitly present in the MF calculations of the phase diagram in the strong-coupling region as well [cf. Eqs. (30),(31)]. This transformation is the reason that explains that the model is (partly) analytically tractable. The interest of finding reliable analytical approaches to strongly coupled fermion systems need not to be stressed.

The fermion propagator $\langle\psi_x\overline{\psi}_y\rangle$ is given by the expectation value of the inverse fermion matrix, which in a large-y expansion becomes

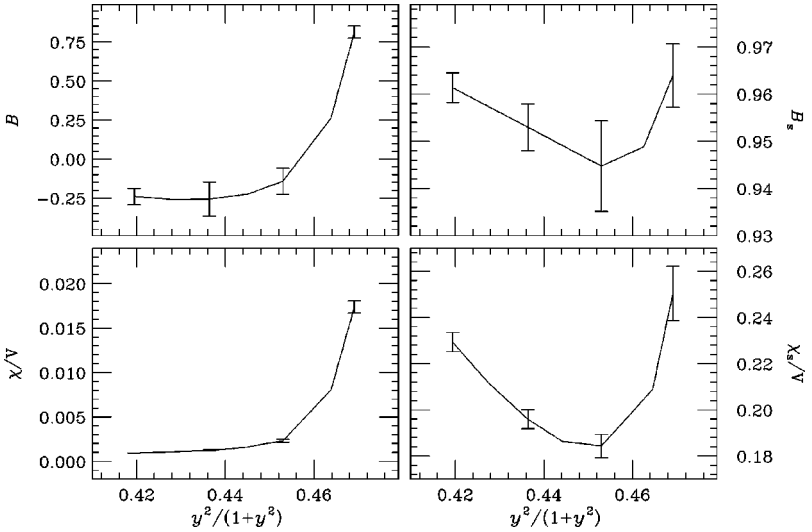

FIG. 5. Binder cumulants and susceptibilities when crossing the AFM(W)-FI transition line at $k=-1.6$.

$$\langle \psi_x \overline{\psi}_y \rangle = \langle M^{-1}_{xy} \rangle = \left\langle \frac{1}{y} \left(1 - \frac{1}{y} K(\boldsymbol{\phi}\cdot\boldsymbol{\tau}) + \frac{1}{y^2} K(\boldsymbol{\phi}\cdot\boldsymbol{\tau}) K(\boldsymbol{\phi}\cdot\tau) - \ldots \right)_{xy} \right\rangle . \tag{64}$$

This can be viewed as a sum over paths of increasing length connecting x and y (recall that K is a nearest-neighbor matrix).

In the FM(S) phase, there is a non-zero magnetization $v = |\langle \boldsymbol{\phi} \rangle|$. Expectation values of products of $\boldsymbol{\phi}$ fields on different sites are replaced by the appropriate powers of v. Corrections to this approximation as well as contributions from paths visiting a given site more than once are of higher order in $1/d$ and are ignored at the MF level. The series (64) can thus be resummed and one finds a propagator

$$\langle \psi \overline{\psi} \rangle_{FM(S)} = \frac{1/v}{K + y/v} \tag{65}$$

which is that of a fermion with a mass y/v. Note that, since $v<1$, this is a huge mass if y is large. The propagator for the original fermion, before the change of variables (60),(61), corresponds to the same physical particle; the only difference is in the wave function renormalization.

In the PM(S) phase, $v=0$, so at the MF level the fermion would be infinitely massive, or in other words, non-propagating. Beyond this naive MF level, however, a large but finite mass will be found. This is due to the next-to-leading contributions to the series (64). The dominant terms are now those involving the expectation value for the nearest-neighbor energy $z^2 \equiv \langle \boldsymbol{\phi}_x \cdot \boldsymbol{\phi}_{x+\hat{\mu}} \rangle$, which is of order $1/2d$ and therefore absent at the MF level. The resummation of contributions in Eq. (64) now leads to a fermion propagator with a mass y/z, which is even larger than the mass of the fermion in the FM(S) phase. However, one should keep in mind that the above arguments only hold deep in the PMS phase, far from the phase transition lines which, for large y, are second order.

The conclusion of this analysis, which is similar to that in (chiral) Yukawa models in the Electroweak theory [24], is that the elementary fermion excitations in the large-y region are very heavy (hence essentially non-propagating), and therefore play no role in the spectrum of light excitations. This holds even more strongly in the PMS phase than in the FM(S) phase.

B. Fermionic excitations in the AFM(S) phase

Here our point of departure is again the form of the action (63), which is tailored for studying the large-y behavior. In the AFM(S) phase, we have a staggered expectation value for the $\boldsymbol{\phi}$ field at the MF level, which can be taken in the 3-direction,

$$\boldsymbol{\phi}_x = \epsilon_x v \begin{pmatrix} 0 \\ 0 \\ 1 \end{pmatrix} \tag{66}$$

[with $\epsilon_x = (-1)^{x_1+x_2+x_3}$]. Hence

$$(\boldsymbol{\phi}_x \cdot \boldsymbol{\tau}) \psi_x = \begin{pmatrix} v \epsilon_x \psi^{(1)}_x \\ -v \epsilon_x \psi^{(2)}_x \end{pmatrix}, \tag{67}$$

where $\psi^{(i)}_x$, $i=1,2$ labels the two *flavors* in ψ_x. So after the change of variables (60),(61) the kinetic operator in Eq. (63) is still diagonal in flavor. The only effect of the new variables is to change the lattice Dirac operator from Eq. (12) to

$$v \epsilon_y \tau_3 K_{xy} .$$

Due to this diagonal structure in flavor space, we can concentrate on one flavor, say $\psi^{(1)}$; the other flavor is obtained by taking $-v$ instead of v. In Fourier space, the kinetic term for $\psi^{(1)}$ is given by

$$-iv \not{\sin} p \, \delta_{p, q \pm \pi}, \tag{68}$$

where

$$\not{\sin} p = \sum_\mu \sigma_\mu \sin p_\mu , \tag{69}$$

$$\delta_{p, q \pm \pi} = \prod_\mu \delta_{p_\mu, q_\mu + \pi \bmod 2\pi} . \tag{70}$$

So we obtain for the inverse of the MF propagator in the AFM(S) phase,

$$M_{p,q} = -iv \not{\sin} p \, \delta_{p, q \pm \pi} + y \, \delta_{p,q}, \tag{71}$$

or, in matrix notation for the subspace of the modes coupled in Eq. (71), p and $p \pm (\pi, \pi, \pi)$,

$$M_{p, p \pm (\pi,\pi,\pi)} = \begin{pmatrix} y & -iv \not{\sin} p \\ iv \not{\sin} p & y \end{pmatrix}. \tag{72}$$

To find the quasiparticle excitations in the AFM(S) phase we diagonalize the fermionic part of the action (72). One obtains

$$S = \int_p \overline{\psi}(p) (y - v \not{\sin} p) \psi(p), \tag{73}$$

where

$$\psi(p) = \frac{1}{\sqrt{2}} [\psi^{(1)}(p) + i \psi^{(1)}(p+\pi)],$$

or, in *position* space,

$$\psi_x = \frac{1}{\sqrt{2}}[\psi_x^{(1)} + i\epsilon_x \psi_x^{(1)}].$$

The momentum space propagator corresponding to Eq. (73) is thus

$$S(p) = \frac{1}{y - v\not{s}\not{i}\not{n}p} = \frac{y + v\not{s}\not{i}\not{n}p}{y^2 - v^2 \sum_\lambda \sin^2 p_\lambda}. \tag{74}$$

Since we are working in imaginary time, one would expect quasiparticle poles in $S(p)$ to appear at negative values of p^2. The unusual relative minus sign in the denominator (74) therefore does not seem to allow for a quasiparticle interpretation, at first sight.

However, Eq. (74) suggests the possibility of light excitations with a relativistic dispersion relation around momenta $(\pm\pi/2, \pm\pi/2, \pm\pi/2)$. To see this, consider the denominator in Eq. (74) for small $k_\mu = p_\mu \pm \pi/2$:

$$y^2 - v^2 \sum_\lambda \sin^2 p_\lambda = (y^2 - v^2 d) + v^2 \sum_\lambda k_\lambda^2 + \mathcal{O}(k^4), \tag{75}$$

where $d=3$ is the space-time dimension. As long as we are at large enough y, such that $y^2 > dv^2$ (recall $v^2 < 1$), this dispersion relation corresponds to a relativistic excitation with $m^2 = (y^2 - dv^2)/v^2$, in this naive MF calculation. Several comments are in order:

(1) For $v=0$, we recover the MF result for the PMS phase: the kinetic term in Eq. (75) is suppressed.

(2) At the MF level, only for $(y^2 - dv^2)$ small enough compared to v^2 these fermionic excitations, $(\boldsymbol{\tau}\cdot\boldsymbol{\phi})\psi$, can propagate easily. Since $v^2 < 1$, this can only happen for y^2 not too large.

(3) These would-be excitations are characteristic of the AFM(S) phase. Let us recall that in the PMS phase no *light* fermionic excitations have been identified at the MF level.

C. Light bound states in the PMS phase

We have seen above that the fermionic excitations in the PMS phase are very heavy. We will now show that there are bound states of elementary fermions, however, which are light. This is done by means of a MF calculation of the double-chain type [25].

Consider the propagator for a fermion pair $\psi_x \psi_x$,

$$\langle \psi^\alpha_{x,i} \psi^\beta_{x,j} \overline{\psi}^\lambda_{y,k} \overline{\psi}^\rho_{y,l} \rangle = \langle M^{-1}_{x,\beta,j;y,\lambda,k} M^{-1}_{x,\alpha,i;y,\rho,l} \rangle - \langle M^{-1}_{x,\alpha,i;y,\lambda,k} M^{-1}_{x,\beta,j;y,\rho,l} \rangle. \tag{76}$$

Here M^{-1} is the single-fermion propagator, $\alpha,\beta,\lambda,\rho$ are Dirac indices, and i,j,k,l are flavor indices. Thus, this propagator is really a 16×16 matrix. For the moment we keep all these indices as they are; later on we will discuss how pairs of them decompose into quantum numbers for the composite state.

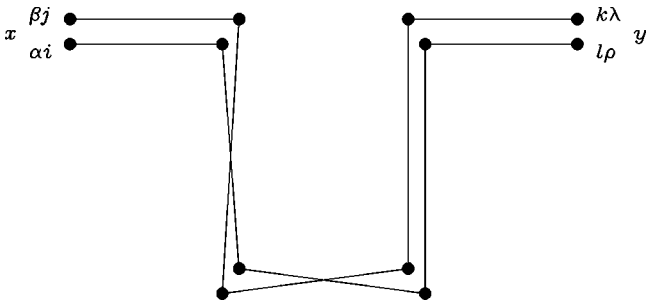

FIG. 6. A typical double-chain diagram, connecting sites x and y. The chains are parallel in position space.

Let us concentrate on the first $\langle M^{-1} M^{-1} \rangle$ term in Eq. (76). Using the $1/y$ expansion of M^{-1} as before, we find the series

$$\langle M^{-1}_{x,\beta,j;y,\lambda,k} M^{-1}_{x,\alpha,i;y,\rho,l} \rangle = \sum_{N,N'=0}^{\infty} \left\langle \left[\frac{\phi}{y} \left(K \frac{\phi}{y} \right)^N \right]_{x,\beta,j;y,\lambda,k} \left[\frac{\phi}{y} \left(K \frac{\phi}{y} \right)^{N'} \right]_{x,\alpha,i;y,\rho,l} \right\rangle, \tag{77}$$

where we have written ϕ as a shorthand for $(\boldsymbol{\phi}\cdot\boldsymbol{\tau})$. It is clear that only terms with $N+N'$ even survive in a paramagnetic phase, due to the $\boldsymbol{\phi} \to -\boldsymbol{\phi}$ symmetry, thus a factor $(-1)^{N+N'}$ has been dropped. Since the matrix K connects nearest-neighbor sites only, each term in this series can be seen to represent a product of two paths (chains) of lengths N and N' respectively, connecting site x with site y [so, if the ''distance'' between x and y is even(odd), both N and N' will be even(odd)].

We will attempt to sum the complete series, to leading order in $1/d$, where $d = 1+2 = 3$ is the Euclidean space-time dimension. For this, we need the spin-spin propagator, which in this approximation is extremely short ranged

$$\langle \phi^a_x \phi^b_x \rangle = \frac{1}{3} \delta^{ab}. \tag{78}$$

Expectation values of the type $\langle \boldsymbol{\phi}_x \cdot \boldsymbol{\phi}_{x+\hat{\mu}} \rangle$ are of order $1/d$, and others are suppressed even more strongly. Thus, assuming Eq. (78), we observe that any term in the series which contains $\boldsymbol{\phi}_x$ for a given site x only once or an odd number of times will vanish due to $\langle \boldsymbol{\phi} \rangle = 0$. When the site is visited twice, it follows from $\boldsymbol{\phi}^2 = 1$ that the contribution from the $\boldsymbol{\phi}$ fields is proportional to $\frac{1}{3}\delta^{ab}$. Thus each site along the chains connecting x and y must be visited an even number of times. One class of diagrams fulfilling this requirement consists of the so-called ''double-chain'' diagrams, where the propagation of both fermions between x and y follows the same path in position space (see Fig. 6). As was convincingly argued in Ref. [25], this class saturates the dominant diagrams in the $1/d$ expansion. Indeed, one can easily check by concrete examples, how deviations from double-chain behavior induce additional powers of $1/d$. We shall also assume that these double chains are self-avoiding (this is allowed at first order in $1/d$).

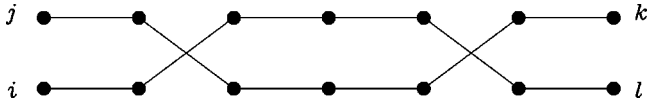

FIG. 7. A matrix-product term contributing to the flavor structure.

Our task is thus to sum up all double chain diagrams connecting x and y. Let us first consider the flavor structure. Using Eq. (78) one finds that

$$\langle(\boldsymbol{\phi}_x\cdot\boldsymbol{\tau})_{jk}(\boldsymbol{\phi}_x\cdot\boldsymbol{\tau})_{il}\rangle=\frac{1}{3}\sum_a \tau^a_{jk}\tau^a_{il}=\frac{1}{3}(-\delta_{jk}\delta_{il}+2\delta_{jl}\delta_{ik}). \tag{79}$$

From this and from the ultra-local correlations we are considering [cf. Eq. (78)], it follows that the product of $2(N+1)$ factors of $(\boldsymbol{\phi}\cdot\boldsymbol{\tau})$ along a double chain of length N visiting the points $x=x_0,x_1,\ldots,y=x_N$ [cf. Eq. (77)] is

$$\left\langle\left[\prod_{n=0}^{N}(\boldsymbol{\phi}_{x_n}\cdot\boldsymbol{\tau})\right]_{x,j;y,k}\left[\prod_{n'=0}^{N}(\boldsymbol{\phi}_{x_{n'}}\cdot\boldsymbol{\tau})\right]_{x,i;y,l}\right\rangle = P\,\delta_{jk}\delta_{il}+Q\,\delta_{jl}\delta_{ik}. \tag{80}$$

To calculate P and Q, it is convenient to represent the general term contributing to the above matrix product as in Fig. 7. A graph contributing to $\delta_{jk}\delta_{il}$ will have an even number of crossings, while diagrams contributing to $\delta_{jl}\delta_{ik}$ jump an odd number of times. Each crossing contributes a factor $\frac{2}{3}$, while non-crossings yield factors $-\frac{1}{3}$ [cf. Eq. (79)]. Now, P and Q can be easily obtained using binomial summation:

$$\left\langle\left[\prod_{n=0}^{N}(\boldsymbol{\phi}_{x_n}\cdot\boldsymbol{\tau})\right]_{x,j;y,k}\left[\prod_{n'=0}^{N}(\boldsymbol{\phi}_{x_{n'}}\cdot\boldsymbol{\tau})\right]_{x,i;y,l}\right\rangle = \left(\frac{1}{3}\right)^N\frac{1}{2}(\delta_{jk}\delta_{il}+\delta_{jl}\delta_{ik})+(-1)^N\frac{1}{2}(\delta_{jk}\delta_{il}-\delta_{jl}\delta_{ik}), \tag{81}$$

where we have separated in a term symmetric under $(ji)\leftrightarrow(ij)$ and an antisymmetric one (this will be needed for separating the contribution to different quantum numbers). It is remarkable that the flavor contribution only depends on the double-chain length, but not on its shape. This allows for a total factorization between flavor and Dirac indices.

Next, consider the Dirac structure. Let us denote μ_n the lattice unit vector given by $x_{n+1}-x_n$. At each step of the double chain the first line of it contributes a matrix $\sigma^{\mu_n}_{\beta_n\lambda_n}$, while from the second line we have $\sigma^{\mu_n}_{\alpha_n\rho_n}$. The Dirac indices verify $\beta_0=0$, $\alpha_0=0$ and $\lambda_{N-1}=\lambda,\rho_{N-1}=\rho$, in addition to the matrix product conditions: $\lambda_n=\beta_{n+1},\rho_n=\alpha_{n+1}$. So, we have factors

$$K^{\mu_n}_{x_nx_{n+1}}K^{\mu_n}_{x_nx_{n+1}}\sigma^{\mu_n}_{\beta_n\lambda_n}\sigma^{\mu_n}_{\alpha_n\rho_n}, \tag{82}$$

along the double chain, where

$$K^{\mu}_{xy}=\frac{1}{2}(\delta_{y,x+\hat{\mu}}-\delta_{y,x-\hat{\mu}}). \tag{83}$$

One readily finds that

$$A^{\mu}_{xy}\equiv 4K^{\mu}_{xy}K^{\mu}_{xy}=(\delta_{y,x+\hat{\mu}}+\delta_{y,x-\hat{\mu}}). \tag{84}$$

Thus, we need to calculate

$$\sum_{\{\mu_n\}}\left[\prod_n\frac{1}{4}A^{\mu_n}\sigma^{\mu_n}\otimes\sigma^{\mu_n}\right]_{x,\beta,\alpha;y,\lambda,\rho}, \tag{85}$$

where the sum is extended to all the lattice paths (denoted by $\{\mu_n\}$) of length N connecting x and y. Now, we can extend the sum to *all* length-N lattice paths starting at x, because paths not connecting x to y will contribute a zero xy entry. This can be also understood by realizing that once the chain has arrived at x_i, there are $2d$ possible directions to continue the chain. These are added up by summing Eq. (82) over μ. At the next site, we do the same for the next step along the chain. The contributions of all double chains are therefore added up when we take the product of these μ sums along the chain. Corrections due to backtracking $(2d\rightarrow 2d-1)$ are down by $1/d$.

So we need to calculate powers of the matrix

$$\frac{1}{4}\sum_\mu A^\mu\sigma^\mu\otimes\sigma^\mu. \tag{86}$$

One way to do that is to write it out explicitly as a 4×4 matrix in the space spanned by the vectors $(\beta,\lambda)=(1,1)$, (2,2), (1,2) and (2,1), in that order. One finds that it equals

$$\frac{1}{4}\begin{pmatrix} A^3 & A^1-A^2 & 0 & 0\\ A^1-A^2 & A^3 & 0 & 0\\ 0 & 0 & -A^3 & A^1+A^2\\ 0 & 0 & A^1+A^2 & -A^3\end{pmatrix}. \tag{87}$$

It can be diagonalized in this 4×4 space. The eigenvalues, up to the factor 1/4, are found to be

$$\lambda^\mu=A-2A^\mu\quad(\mu=1,2,3), \tag{88}$$

$$\lambda^4=-A, \tag{89}$$

where

$$A=\sum_{\mu=1}^{3}A^\mu=\Box+2d, \tag{90}$$

and $\Box$ is the lattice discretization of the d'Alembertian $\Sigma_\mu\partial_\mu\partial_\mu$. The Nth power [see Eq. (85)] of the matrix (86) is now easy to calculate.

In order to collect the factors and sum up the contributions, let us go back to Eq. (76). We see that we need to antisymmetrize each term in $\langle M^{-1}M^{-1}\rangle$ with respect to the simultaneous interchange of α,i with β,j. This gives a sum of two terms, one symmetric in $\alpha\leftrightarrow\beta$ and antisymmetric in $i\leftrightarrow j$ (corresponding to a composite state which is a Dirac

vector and a flavor singlet), and one vice versa (singlet in Dirac space, vector in flavor space). Note that Eq. (81) has already been written as a sum of symmetric and antisymmetric terms. The symmetric and antisymmetric parts of the Dirac structure correspond to Eqs. (88) and (89), respectively.

Collecting the various factors, we can carry out the geometric sum over N in Eq. (76) and we find the following propagators for the composite states:

a Dirac vector–flavor singlet with propagator

$$\frac{8\,\delta^{\mu\nu}}{-\Box+2A^{\mu}-4y^2-2d} \tag{91}$$

where a,b are the Dirac vector indices

a Dirac singlet—flavor vector with propagator

$$\frac{-8\,\delta_{IJ}}{-\Box-12y^2-2d} \tag{92}$$

where I,J are the flavor vector indices.

These have the form of massive bosonic propagators, up to the following caveat (of course, higher order corrections in $1/d$ may induce shifts in the precise location of the poles, as well as their residues).

The propagators in Eq. (91) contain the matrix $2A^{\mu}$ in the denominator. However, this term must be ignored since it is sub-dominant in $1/d$, compared with the (lattice) d'Alembertian $\Box$.

The numerator of the propagator (91) carries a delta function only, instead of the usual tensor structure $\delta_{\mu\nu}-\partial_{\mu}\partial_{\nu}/m^2$. This is also an artifact of the $1/d$ approximation.

Notice also that the terms which would play the role of a mass squared in the denominators have an apparently wrong sign. However, it is easy to check that the composite field $\epsilon_x\psi_x\psi_x$ [where $\epsilon_x=(-1)^{\Sigma_\mu x_\mu}$ as usual] does lead to a massive Dirac singlet—flavor vector propagator with mass squared $m^2_{(0,1)}=12y^2-2d=12y^2-6$. Similarly, one obtains a massive Dirac vector–flavor singlet with a mass squared $m^2_{(1,0)}=4y^2-2d=4y^2-6$. We thus conclude that the right interpolating field is $\epsilon_x\psi_x\psi_x$ [25].

The conclusion is that we find massive bound states of fermions in the PMS phase. They are bound by the strong interactions with the spin waves. These composites are lighter than the elementary fermions in this phase, when y moves away from the value ∞.

VI. CONCLUSIONS

In this work we have concerned ourselves with the general features and the analytical and numerical study of the lattice model given by expression (2).

From the numerical side, we have developed a new method that exactly solves the technical problem related to the length-1 constraint on the spin variable.

The model describes qualitatively some of the properties of the doped copper oxide compounds [1,2] and has interesting properties in the strong coupling regime. In fact, at the mean-field level, no light fermion excitations have been identified in the FM(S) and PMS phases. However, in the AFM(S) phase, see Sec. V B, light excitations around momenta $(\pm\pi/2,\pm\pi/2,\pm\pi/2)$ have been found. Its possible relevance for the doped copper oxide compounds has been noticed in [1,2,4].

Concerning the PMS phase (see Fig. 1), the situation is also interesting. While the fermionic excitations in this phase are very heavy (see Sec. V A) we have found light bound states of fermions (see Sec. V C). They are spin singlet bosonic states of charged fermions bound by the strong interactions with the spin waves. A similar result has been found in the model of Ref. [25].

The next step is to study the model in the presence of chemical potential and at finite temperature (after going to $3+1$ dimensions). In fact, as we have proved in Sec. II, the fermion determinant is still real after the introduction of the chemical potential.

ACKNOWLEDGMENTS

We are indebted to L.A. Fernández for very helpful remarks and stimulating discussions. We also acknowledge interesting discussions with A. Cruz, Ph. de Forcrand, M.A. Stephanov, and A. Tarancón. We thank the RTNN collaboration for computing facilities. This work is financially supported by CICYT (Spain), projects AEN 96-1670, AEN 96-1674, AEN 97-1680 and by Acción Integrada Hispano-Francesa HF1996-0022.

[1] J.L. Alonso, Ph. Boucaud, V. Martín-Mayor, and A.J. van der Sijs, Europhys. Lett. **42**, 541 (1998).

[2] J.L. Alonso, Ph. Boucaud, V. Martín-Mayor, and A.J. van der Sijs, Nucl. Phys. B (Proc. Suppl.) **63**, 658 (1998).

[3] G. Parisi, Nucl. Phys. **B205**, 337 (1982); E. Abdalla, Phys. Rev. D **41**, 571 (1990).

[4] A similar result has been found by A.V. Chubukov and D.K. Morr, Phys. Rep. **288**, 355 (1997).

[5] K. Wilson, in *New Phenomena in Sub-Nuclear Physics* (Erice, 1975), edited by A. Zichichi (Plenum, New York, 1997); L.H. Karsten and J. Smit, Nucl. Phys. **B183**, 103 (1981); H.B. Nielsen and Ninomiya, *ibid.* **B185**, 20 (1981); **B193**, 173 (1981); **B195**, 541(E) (1982).

[6] A.K. De and J. Jersák, in *Heavy Flavors*, edited by A. Buras and M. Lindner (World Scientific, Singapore, 1992).

[7] T.W. Appelquist, M. Bowick, D. Karabali, and L.C.R. Wijewardhana, Phys. Rev. D **33**, 3704 (1986).

[8] For a review, see F. Karsch, in *Quark Gluon Plasma*, edited by R.C. Hwa (World Scientific, Singapore, 1990).

[9] See, e.g., J. Shigemitsu, Nucl. Phys. B (Proc. Suppl.) **20**, 515 (1991); W. Bock, *et al.*, Nucl. Phys. **B344**, 207 (1990).

[10] J.-M. Drouffe and J.-B. Zuber, Phys. Rep. **102**, 1 (1983); R. Balian, J.M. Drouffe, and C. Itzykson, Phys. Rev. D **10**, 3376 (1974); **11**, 2104 (1975); **19**, 2514(E) (1979).

[11] J.L. Alonso, Ph. Boucaud, F. Lesmes, and E. Rivas, Phys. Lett. B **329**, 75 (1994).
[12] J.L. Alonso, Ph. Boucaud, F. Lesmes, and A.J. van der Sijs, Nucl. Phys. **B457**, 175 (1995); **B472**, 738(E) (1996).
[13] V. Branchina, H. Mohrbach, and J. Polonyi, Phys. Rev. D **60**, 045006 (1999); **60**, 045007 (1999).
[14] K. Farakos, K. Kajantie, K. Rummukainen, and M. Shaposhnikov, Nucl. Phys. **B442**, 317 (1995); P. Arnold, Phys. Rev. D **55**, 7781 (1997).
[15] R.T. Scalettar, D.J. Scalapino, and R.L. Sugar, Phys. Rev. B **34**, 7911 (1986); S. Duane, A.D. Kennedy, B.J. Pendleton, and D. Roweth, Phys. Lett. B **195**, 216 (1987).
[16] G. Batrouni *et al.*, Phys. Rev. D **32**, 2736 (1986); S. Gottlieb, W. Liu, D. Toussaint, and R.L. Sugar, *ibid.* **35**, 2531 (1987).
[17] I. Montvay and G. Münster, *Quantum Fields on a Lattice* (Cambridge University Press, Cambridge, England, 1994); H.J. Rothe, *Lattice Gauge Theories – An Introduction* (World Scientific, Singapore, 1992).
[18] H. Goldstein, *Classical Mechanics* (Addison-Wesley, Redwood City, CA, 1959).
[19] U. Wolff, Phys. Rev. Lett. **62**, 361 (1989).
[20] H. G. Ballesteros, L. A. Fernández, V. Martín-Mayor, and A. Muñoz Sudupe, Phys. Lett. B **387**, 125 (1996).
[21] M. Falcioni, E. Marinari, M. L. Paciello, G. Parisi, and B. Taglienti, Phys. Lett. **108B**, 331 (1982); A. M. Ferrenberg and R. H. Swendsen, Phys. Rev. Lett. **61**, 2635 (1988).
[22] J. L. Alonso *et al.*, Phys. Rev. B **53**, 2537 (1996); H. G. Ballesteros, L. A. Fernández, V. Martín-Mayor, and A. Muñoz Sudupe, Phys. Lett. B **378**, 207 (1996).
[23] R. Gupta *et al.*, Phys. Rev. D **40**, 2072 (1989).
[24] J. Smit, Nucl. Phys. B (Proc. Suppl.) **9**, 579 (1989); M.F.L. Golterman, D.N. Petcher, and J. Smit, Nucl. Phys. **B370**, 51 (1992).
[25] M.A. Stephanov and M.M. Tsypin, Phys. Lett. B **236**, 344 (1990); M.A. Stephanov, *ibid.* **266**, 447 (1991).